NACA RM L51C16

NACA

RESEARCH MEMORANDUM

INVESTIGATION OF THE EFFECTS OF TWIST AND CAMBER ON THE AERODYNAMIC CHARACTERISTICS OF A 50° 38' SWEPTBACK WING OF ASPECT RATIO 2.98

TRANSONIC-BUMP METHOD

By Kenneth P. Spreemann and William J. Alford, Jr.

Langley Aeronautical Laboratory
Langley Field, Va.

NATIONAL ADVISORY COMMITTEE
FOR AERONAUTICS

WASHINGTON

August 27, 1951

NACA RM L51C16

NATIONAL ADVISORY COMMITTEE FOR AERONAUTICS

RESEARCH MEMORANDUM

INVESTIGATION OF THE EFFECTS OF TWIST AND CAMBER ON THE AERODYNAMIC CHARACTERISTICS OF A 50° 38' SWEPTBACK WING OF ASPECT RATIO 2.98

TRANSONIC-BUMP METHOD

By Kenneth P. Spreemann and William J. Alford, Jr.

SUMMARY

An investigation of two semispan wings of identical plan form (swept back 50° 38') was conducted in the Langley high-speed 7- by 10-foot tunnel over a Mach number range of 0.68 to 1.15 by means of the transonic-bump technique to determine the effects of twist and camber on the aerodynamic characteristics of a sweptback wing. This paper presents the results of the investigation of wing-alone and wing-fuselage configurations of the two wings; one was an untwisted and uncambered wing and the other incorporated twist and camber designed to give uniform load at a lift coefficient of 0.25 at a Mach number of 1.10. The semispan wings had their quarter-chord lines swept back 50° 38', aspect ratios 2.98, taper ratios 0.45, and modified NACA 64A-series airfoil sections tapered in thickness. Lift, drag, pitching moment, and root bending moment were obtained for these configurations.

The results show that, for lift coefficients above 0.10, the lift-drag ratios were increased throughout the Mach number range investigated by twisting and cambering the wing. No significantly large changes in lift-curve slope, minimum drag, or movement of the aerodynamic-center location were occasioned by twisting and cambering the wing. Camber and twist resulted in negative displacements of the pitching-moment curve, particularly for the wing-fuselage combination. The pitching moment at zero lift generally showed rather small variations with Mach number.

INTRODUCTION

In the transonic and supersonic speed range one of the promising configurations from a compromise between aerodynamic and structural requirements is the swept wing of low aspect ratio with thin airfoil section. A wing of this type has the advantage of low drag at zero lift but this gain in performance is partly offset by high drag due to lift. Previous investigations at subsonic and supersonic speeds have shown that the lift-drag characteristics can be improved by twisting and cambering the wing (references 1 and 2). To secure information through the transonic speed range, two wings were investigated; one was an untwisted, uncambered wing (hereafter referred to as a flat wing) similar to one tested at subsonic and supersonic speeds (references 3 and 4) and the other had the same plan form but incorporated twist and camber designed to give uniform loading at a Mach number of 1.10 and a lift coefficient of 0.25.

This investigation was conducted in the Langley high-speed 7- by 10-foot tunnel over a Mach number range between 0.68 and 1.15 which was obtained by use of the transonic-bump method. Included in the paper are the results of the investigation of the wings-alone and wing-fuselage combinations. Lift, drag, pitching moment, and root bending moment were obtained for these configurations.

COEFFICIENTS AND SYMBOLS

C_L lift coefficient (Twice semispan lift/qS)

C_D drag coefficient (Twice semispan drag/qS)

C_m pitching-moment coefficient referred to $0.25\bar{c}$ (Twice semispan pitching moment/$qS\bar{c}$)

C_B bending-moment coefficient about axis parallel to relative wind in plane of symmetry $\left(\text{Root bending moment}/q\,\frac{S}{2}\,\frac{b}{2}\right)$

q effective dynamic pressure over span of model, pounds per square foot $\left(\frac{1}{2}\rho V^2\right)$

S twice wing area of semispan model, 0.125 square foot

$\bar{c}$ mean aerodynamic chord of wing, 0.215 foot, based on relationship $\frac{2}{S}\int_0^{b/2} c^2\,dy$ (using theoretical tip)

c local wing chord parallel to plane of symmetry, feet

b twice span of semispan model, 0.61 foot

y spanwise distance from plane of symmetry, feet

ρ air density, slugs per cubic foot

V stream velocity over model, feet per second

M effective Mach number $\left(\frac{2}{S}\int_0^{b/2} cM_a\,dy\right)$

M_l local Mach number

M_a average chordwise Mach number

R Reynolds number $(\rho V\bar{c}/\mu)$

μ absolute viscosity, pound-seconds per square foot

α angle of attack of fuselage reference line ($\bar{c}$ is parallel to fuselage reference line), degrees

ϵ angle of wing twist measured relative to fuselage reference line (fig. 1(b)), degrees

d chordwise distance from wing leading edge parallel to plane of symmetry, feet

z camber, feet

L/D lift-drag ratio

$\alpha_{C_L=0}$ angle of attack at zero lift coefficient, degrees

$y_{c.a.l.}$ lateral center of additional loading, percent semispan $\left(100\,\frac{\partial C_B}{\partial C_L}\right)$

C_{m_o} pitching-moment coefficient at zero lift coefficient

$C_{D_{min}}$ minimum drag coefficient

$C_{L_{C_{D_{min}}}}$ lift coefficient at minimum drag coefficient

$(L/D)_{max}$ maximum lift-drag ratio

$C_{L_{(L/D)_{max}}}$ lift coefficient at maximum lift-drag ratio

MODELS AND APPARATUS

The steel wings of the flat and the twisted and cambered semispan models had 50° 38' sweepback of their quarter-chord lines, aspect ratios of 2.98, and taper ratios of 0.45. The airfoil sections of the flat wing perpendicular to the 29.3-percent-chord line, where the 29.3-percent-chord line intersects the streamwise root and tip chords, were NACA $64_{(10)}$A010.9 at the root and NACA $64_{(08)}$A008.1 at the tip. The same 64A-series airfoil thickness distribution was placed around the mean camber surface of the twisted and cambered wing. The maximum streamwise thicknesses were 7.4 percent at the root and 5.6 percent at the tip. Two-view drawings of the flat (untwisted, uncambered) wing-fuselage and the twisted and cambered wing-fuselage models are presented as figures 1(a) and 1(b), respectively. Photographs of the flat wing alone and flat wing-fuselage combination are presented as figures 2(a) and 2(b), respectively. Ordinates of the fuselage used are given in table I.

The twisted and cambered wing was designed to obtain a uniform load distribution at a Mach number of 1.10 and a lift coefficient of 0.25. The theoretical mean-surface coordinates of a wing having uniform load at the design conditions were calculated by the method of reference 5. It was found from cross plots of the computed results that the camber (perpendicular distance above chord line) could be satisfactorily modified to give a linear variation in camber with distance along any constant percent chord. The theoretical camber and the linear camber actually used are presented in figure 3, along with the maximum camber and the angle of wing twist. The chordwise location of the maximum camber was 40.0 percent of the streamwise chord throughout the span. To avoid the impracticably large wing twist at the root, the theoretical twist was modified by using a linear fairing.

Force and moment measurements were made with a strain-gage balance enclosed in the tunnel bump. The lift, drag, pitching moment, and root

bending moment were recorded with recording potentiometers. The angle of attack was measured by means of a slide-wire potentiometer and recorded with a galvanometer.

TESTS

The tests were conducted in the Langley high-speed 7- by 10-foot tunnel by the transonic-bump technique (reference 6). The bump utilized in this investigation was larger than that of reference 6; thus, because of the reduction in bump curvature, the local Mach number gradients were considerably less than those associated with the bump of the aforementioned reference. It was pointed out in reference 6 that the effect of bump curvature and local Mach number gradients on the bump results was to move the aerodynamic-center positions somewhat rearward of positions indicated by sting setups, or by semispan setups employing a flat reflection plane. However, no consistent effects of bump curvature and local Mach number gradients were noticed on the other aerodynamic parameters.

The changes in sweep angle of the quarter-chord line of the model caused by the bump curvature were an increase of 1.0° ahead of the balance center line at the root quarter chord and a decrease of 2.3° behind the balance center line at the tip quarter chord. Typical contours of local Mach number in the vicinity of the model location, obtained from surveys with no model in position, are shown in figure 4. The dashed lines near the root of the wing (fig. 4) represent a local Mach number that is 5 percent below the maximum value and indicate the extent of the bump boundary layer. It is seen that outside the boundary layer there is a local Mach number variation of about 0.01 over the model semispan at the lowest Mach numbers and about 0.05 at the highest Mach numbers. The average chordwise Mach number variation is generally less than 0.015. The effective test Mach number was obtained from additional contour charts similar to those presented in figure 4 from the relationship $M = \int_0^{b/2} cM_a \, dy$. The Mach number range generally extended from 0.68 to 1.15 through an angle-of-attack range from about -9° to 24°.

A gap of about 1/16 inch was maintained between the wing root chord and the bump turntable and a sponge-wiper seal was fastened to the wing butt beneath the surface of the turntable to minimize leakage. The turntable was located flush with the bump surface and supported so as to retain the bump contour at all angles of attack.

Jet-boundary corrections have not been evaluated because the boundary conditions to be satisfied are not rigorously defined. However, inasmuch as the effective flow field was large compared with the span and the chord of the model, the corrections are believed to be small. Corrections due to aeroelastic effects were less than 1.0 percent and were not applied to the data.

The variation of mean test Reynolds number with Mach number is shown in figure 5. The cross-hatched region of this plot indicates the range of Reynolds number caused by variations in the atmospheric conditions during the course of the investigation.

RESULTS AND DISCUSSION

A list of the figures presenting the results follows:

Unless otherwise noted, the discussion is based on the summary curves presented in figures 10 and 11. The slopes presented in these figures have been averaged over a lift-coefficient range of 0 to 0.4. It should be pointed out that in the following discussion the changes in the aerodynamic characteristics of the wing-fuselage combination attributed to wing twist and camber may also include interference effects caused by the change in angle of wing incidence at the wing-fuselage juncture.

Lift Characteristics

The wing-alone lift-curve slopes (fig. 10) were only slightly affected by twisting and cambering the wing, although it may be observed that the variation with Mach number was slightly greater for the twisted and cambered wing. Comparison of the lift-curve slopes for

the two wing-fuselage combinations (fig. 11) shows that twisting and cambering the wing gave increases in lift-curve slopes of 0.002 to 0.004.

The angle of attack for zero lift of the wings alone, $\alpha_{C_L=0}$ (fig. 10) was decreased about 2° throughout the Mach number range by twisting and cambering the wing. In the wing-fuselage comparisons, $\alpha_{C_L=0}$ (fig. 11) was considerably less affected by twisting and cambering the wing (maximum reduction of about 1°). This apparent reduction in the change in $\alpha_{C_L=0}$ may be attributed to the loss in lift caused by the fuselage covering part of the wing where large positive changes in twist are present. It may be noted that the angles of attack for zero lift of the twisted and cambered wing were reasonably constant with Mach number for both wing-alone and wing-fuselage configurations, even though they were not as constant as for the flat wing.

Throughout the Mach number range the lateral centers of additional loading $\left(y_{c.a.l.}\right)$ of the twisted and cambered wing for both wing-alone and wing-fuselage configurations (figs. 10 and 11) were 1.5 to 2.0 percent of the semispan farther outboard than the lateral centers of additional loading of the flat wing.

Drag Characteristics

Twisting and cambering the wing caused only slight changes in the shapes of the drag curves but did shift the curves in such a manner as to cause a given drag value to occur at a higher lift coefficient. The summary curves (figs. 10 and 11) indicate that, at the higher Mach numbers, twisting and cambering the wing gave slightly lower minimum drag coefficients than the flat wing for both wing-alone and wing-fuselage configurations. However, it is possible that asymmetry of flow over the bump may have been responsible for the apparent reduction in $C_{D_{min}}$ of the twisted and cambered wing, inasmuch as calculations of induced drag indicated that $C_{D_{min}}$ of the twisted and cambered wing should be about 0.001 higher than that of the flat wing. The fact that the minimum drag coefficients of the twisted and cambered wing occurred at positive lift coefficients for both wing-alone and wing-fuselage configurations is of particular significance for high-speed flight at low lift coefficients. It should be noted that the minimum drag coefficients of the wing-fuselage combination may be high because of the skin friction and interference drag caused by the additional fuselage surface and the gap between the fuselage and the bump surface. It is particularly noticeable in the basic drag data (figs. 6 and 7) that twisting and cambering the wing was quite effective in reducing the drag due to lift for both wing-alone and wing-fuselage configurations.

Lift-Drag Ratios

Over most of the lift-coefficient range, the lift-drag ratios (figs. 8 and 9) were greatly increased by twisting and cambering the wing. Slight reductions in L/D, due to twist and camber, sometimes occurred at lift coefficients below 0.10. The twisted and cambered wing-alone and wing-fuselage configurations have considerably higher values of $(L/D)_{max}$ (figs. 10 and 11) than the flat wing configurations (30 to 65 percent for wing-alone and 15 to 25 percent for wing-fuselage). Increases in Mach number caused reductions in the values of $(L/D)_{max}$, particularly on the twisted and cambered wing. The large reductions in $(L/D)_{max}$ observed between Mach numbers of 0.92 and 0.97 may be attributed primarily to the rise in $C_{D_{min}}$ in this Mach number range.

The lift coefficient at which $(L/D)_{max}$ occurred usually was slightly higher for the twisted and cambered wing configurations than for the flat wing configurations. Large Mach number effects on C_L for $(L/D)_{max}$ were indicated for all the configurations investigated at Mach numbers between 0.90 and 1.00, except in the case of the twisted and cambered wing-alone configuration, which appeared to be relatively unaffected by Mach number.

Pitching-Moment Characteristics

Comparison of the curves of $\partial C_m/\partial C_L$ (figs. 10 and 11) shows that, in the subsonic Mach number range, twisting and cambering the wing usually resulted in more forward locations of the aerodynamic center for both wing-alone and wing-fuselage configurations. The usual rearward movements of the aerodynamic center that occur in the mixed-flow region at Mach numbers between 0.90 and 1.00 were slightly greater for the twisted and cambered configurations than for the flat wing configurations. It should be noted that the fairings of $\partial C_m/\partial C_L$ at Mach numbers between 0.89 and 0.99 for the wing-fuselage combinations (shown by dashed lines) are somewhat in question because of the lack of test points in what appears to be a very critical region. In general, the aerodynamic-center locations of the twisted and cambered wing configurations were more affected by Mach number than those of the flat wing configurations. The basic pitching-moment data (figs. 6 and 7) indicate that the use of a twisted and cambered wing delayed the unstable break in pitching moment to higher lift coefficients in the lower Mach number range. However, above a Mach number of 0.94 the unstable break in the pitching-moment curves occurred at lower lift coefficients for the twisted and cambered wing than for the flat wing.

It may be observed that these effects were less noticeable for the wing-fuselage combination.

A slight negative value of pitching-moment coefficient at zero lift C_{m_o} (fig. 10) was evidenced by the twisted and cambered wing alone. With the fuselage installed, an increment in C_{m_o} of -0.04 (fig. 11) was observed for the twisted and cambered wing-fuselage configuration at Mach numbers below 0.90 although above a Mach number of 0.90 this increment was noticeably reduced. However, the C_{m_o} variations throughout the Mach number range seemed to be gradual and, therefore, trim changes affected by C_{m_o} would be rather small for either the flat or twisted and cambered wing configurations. At subcritical speeds it can be shown theoretically that the negative increment in C_{m_o} caused by camber is partially offset by the basic twist distributions. It would be expected that with the fuselage installed on the wing the counteracting effect of wing twist would be appreciably reduced because of the large twist gradient enclosed in the fuselage (see fig. 3).

CONCLUSIONS

An investigation of the effect of twist and camber on the aerodynamic characteristics of a sweptback wing indicated the following conclusions:

1. At lift coefficients above 0.10, the twisted and cambered wing gave larger values of lift-drag ratios throughout the Mach number range than the untwisted, uncambered wing.

2. No significantly large changes in lift-curve slope, minimum drag, or movement of the aerodynamic-center location were occasioned by twisting and cambering the wing. Camber and twist resulted in negative displacements of the pitching-moment curves, particularly for the wing-fuselage combination. The pitching moment at zero lift generally showed rather small variations with Mach number.

Langley Aeronautical Laboratory
National Advisory Committee for Aeronautics
Langley Field, Va.

REFERENCES

1. Jones, J. Lloyd, and Demele, Fred A.: Aerodynamic Study of a Wing-Fuselage Combination Employing a Wing Swept Back 63°. - Characteristics throughout the Subsonic Speed Range with the Wing Cambered and Twisted for a Uniform Load at a Lift Coefficient of 0.25. NACA RM A9D25, 1949.

2. Hall, Charles F., and Heitmeyer, John C.: Aerodynamic Study of a Wing-Fuselage Combination Employing a Wing Swept Back 63°. - Characteristics at Supersonic Speeds of a Model with the Wing Twisted and Cambered for Uniform Load. NACA RM A9J24, 1950.

3. Kemp, William B., Jr., Becht, Robert E., and Few, Albert G., Jr.: Stability and Control Characteristics at Low Speed of a $\frac{1}{4}$-Scale Bell X-5 Airplane Model. Longitudinal Stability and Control. NACA RM L9K08, 1950.

4. Morris, Garland J., Kennedy, Robert M., and Silsby, Norman S.: The Effect of Sweepback on the Longitudinal Characteristics at a Mach Number of 1.24 of a $\frac{1}{30}$-Scale Semispan Model of the Bell X-5 Airplane from Tests by the NACA Wing-Flow Method. NACA RM L50I28, 1950.

5. Jones, Robert T.: Estimated Lift-Drag Ratios at Supersonic Speed. NACA TN 1350, 1947.

6. Donlan, Charles J., Myers, Boyd C., II, and Mattson, Axel T.: A Comparison of the Aerodynamic Characteristics at Transonic Speeds of Four Wing-Fuselage Configurations as Determined from Different Test Techniques. NACA RM L50H02, 1950.

Table I
Fuselage and Canopy Ordinates

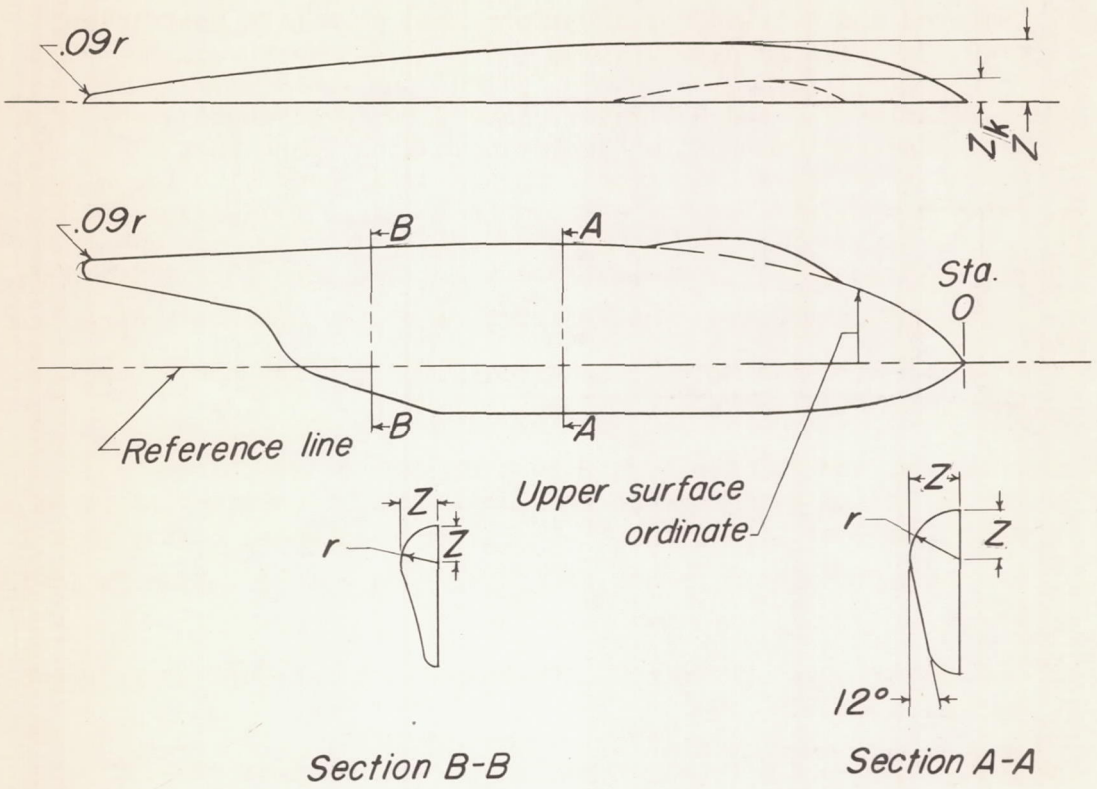

Fuselage Ordinates

Station (in.)	Upper Surface (in.)	Lower Surface (in.)	Z Radius (in.)
0	0	0	0
.47	.47	-.31	.29
.90	.72	-.44	.42
1.97	1.08	-.53	.54
3.05	1.26	-.53	.62
4.12	1.34	-.53	.61
5.20	1.35	-.53	.56
5.95	1.35	-.53	.56
6.27	1.34	-.43	.48
7.35	1.30	-.08	.37
7.56	1.30	.05	.37
7.78	1.30	.40	.37
7.99	1.30	.60	.37
8.42	1.26	.72	.27
9.50	1.21	.89	.15
9.71	1.19	.93	.13
9.98	1.10	1.10	0

r radius, inches

Canopy Ordinates

Station (in.)	Upper Surface (in.)	Z_k (in.)
1.34	.89	0
2.13	1.34	.19
2.51	1.42	.17
3.05	1.42	.11
3.83	1.33	0

NACA

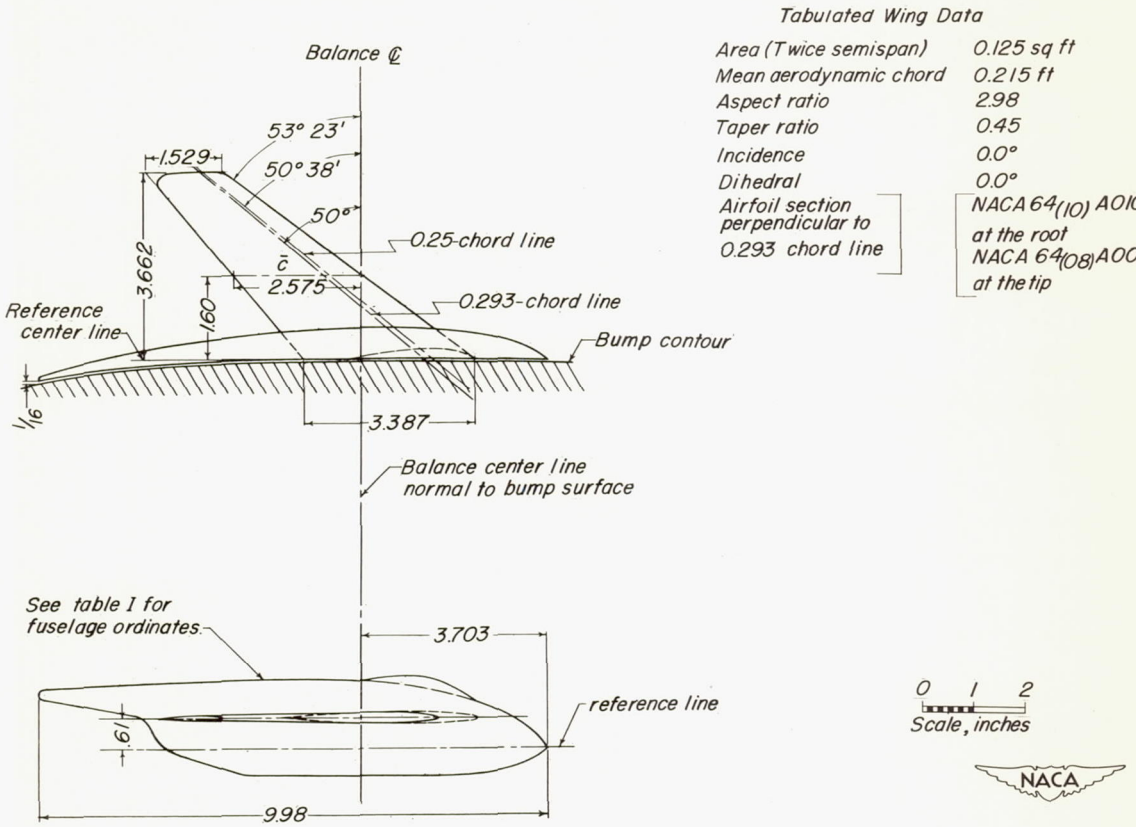

(a) Flat wing-fuselage combination.

Figure 1.- Wing-fuselage combinations with 50° 38' sweptback wings, aspect ratios 2.98, taper ratios 0.45, and modified NACA 64A-series airfoil sections.

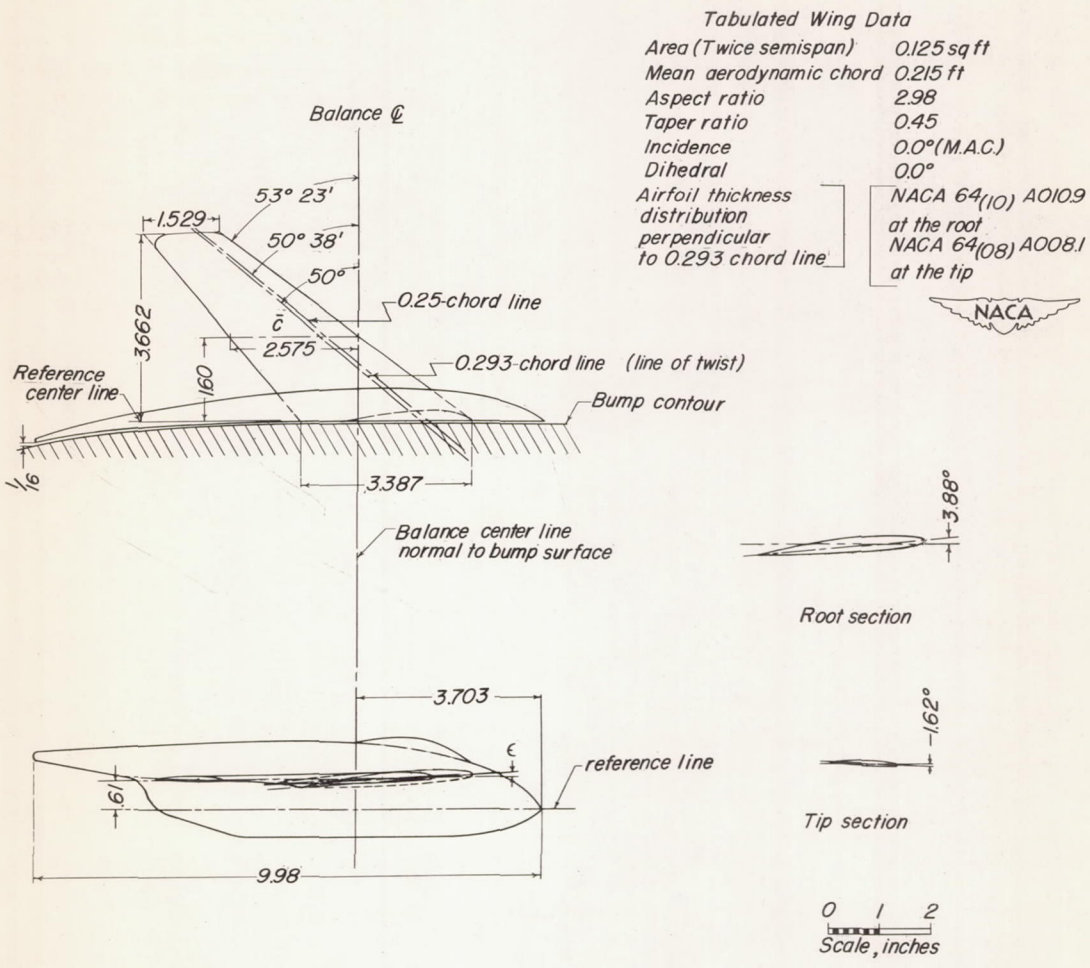

(b) Twisted and cambered wing-fuselage combination.

Figure 1.- Concluded.

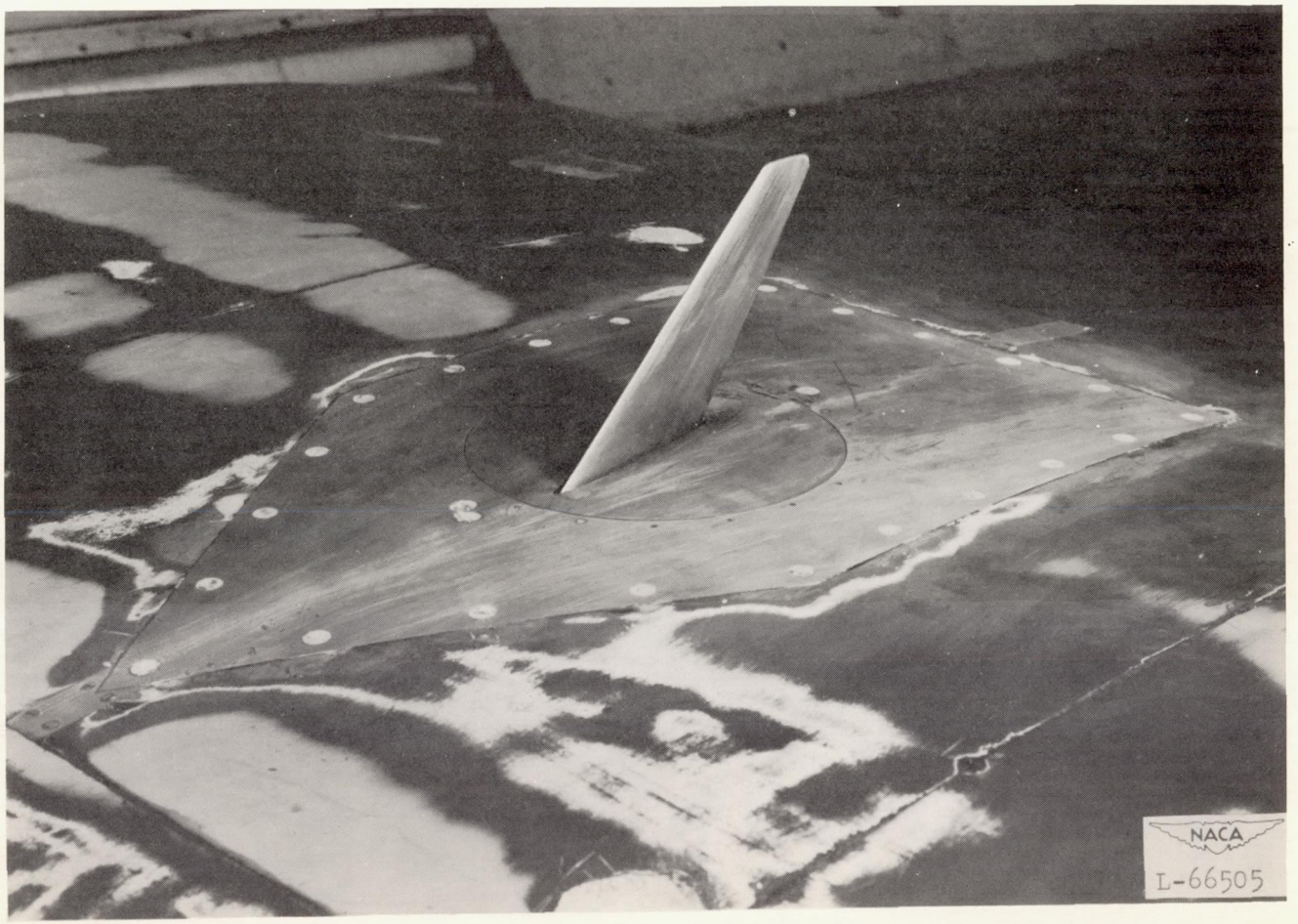

(a) Wing alone.

Figure 2.- Flat wing model with 50° 38' sweptback wing, aspect ratio 2.98, taper ratio 0.45, and modified NACA 64A-series airfoil sections mounted on the transonic bump.

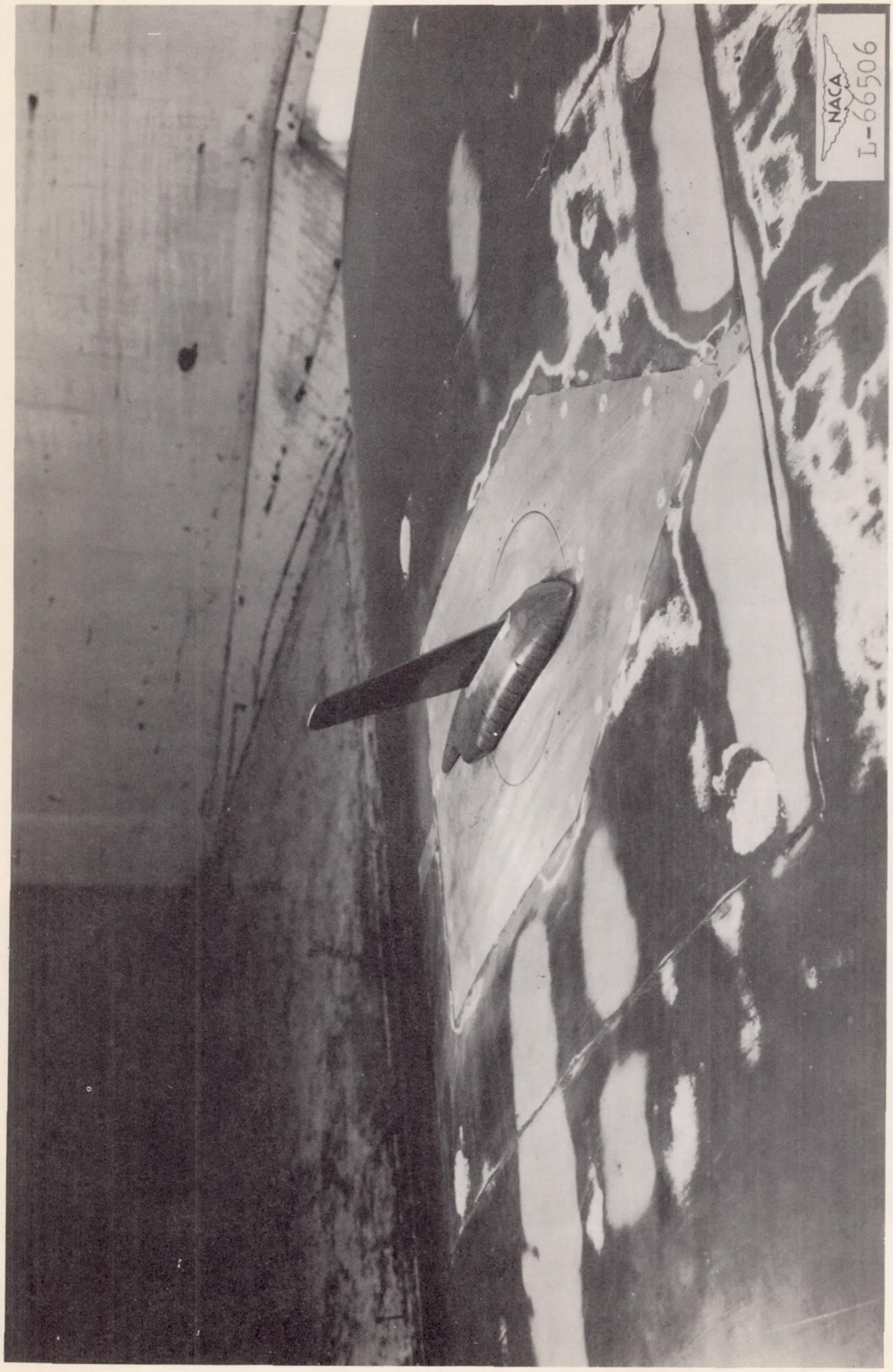

(b) Wing-fuselage combination.

Figure 2.- Concluded.

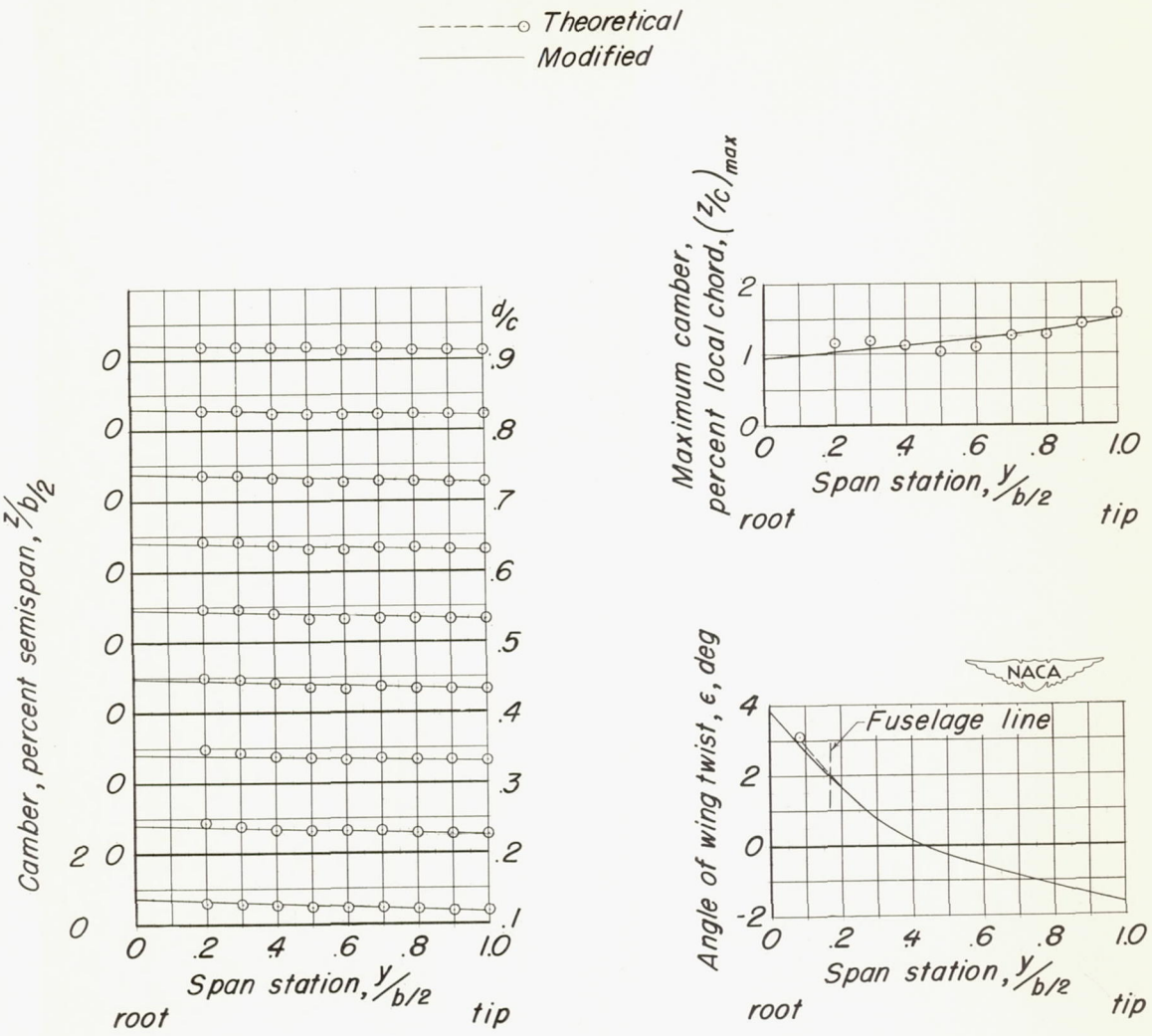

Figure 3.- Spanwise variations of twist and camber of the twisted and cambered wing.

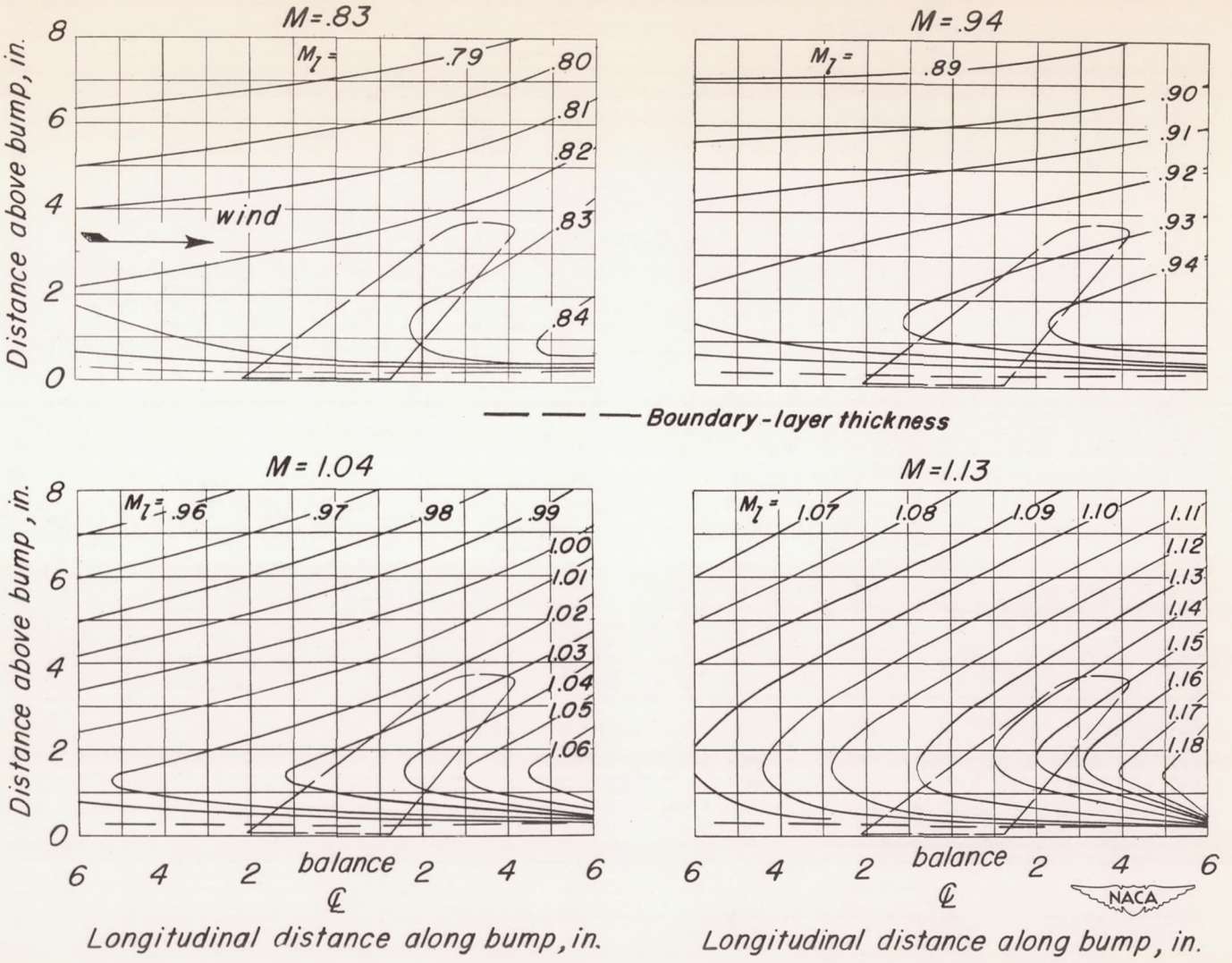

Figure 4.- Typical Mach number contour over transonic bump in region of model location.

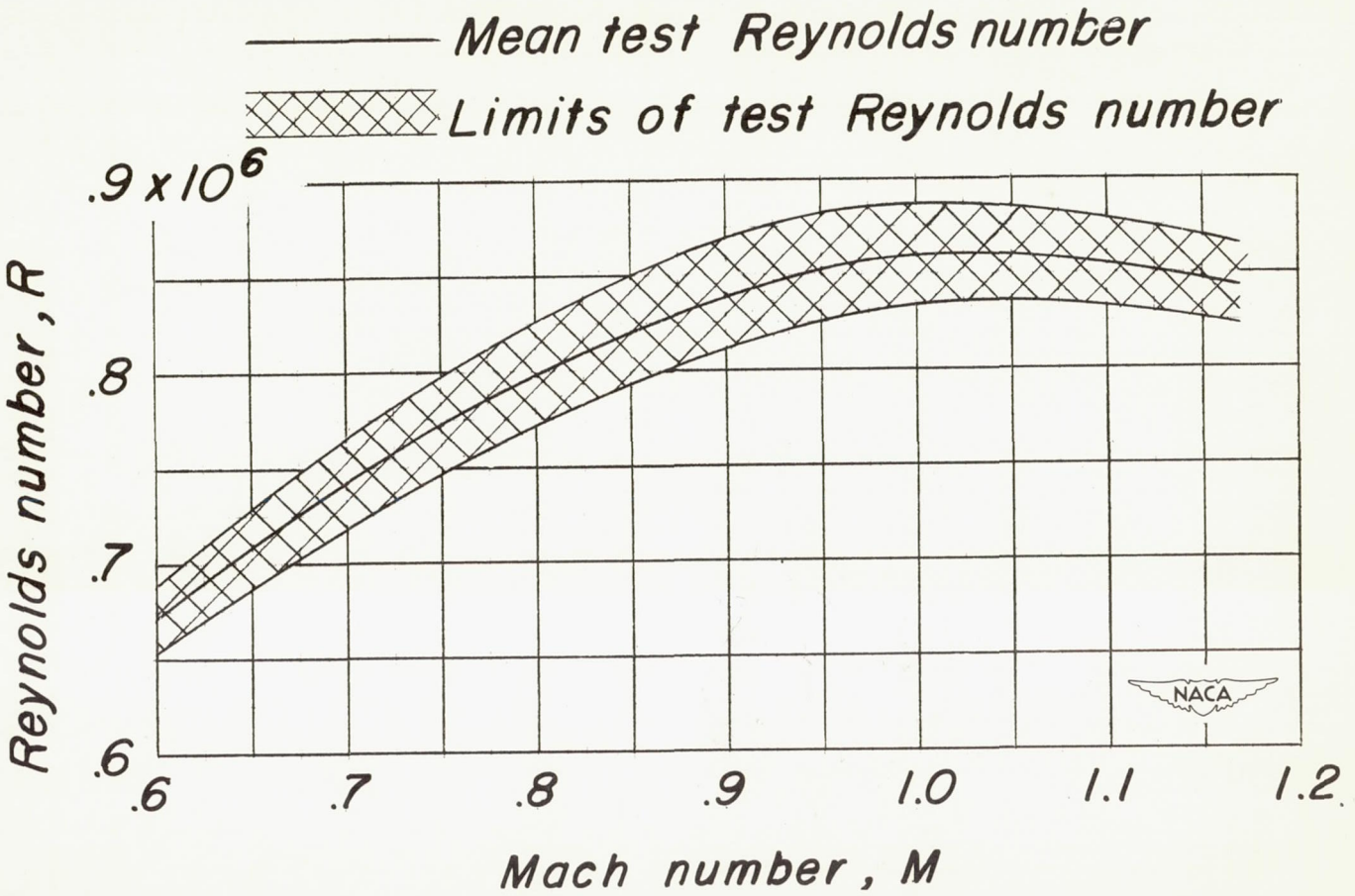

Figure 5.- Variation of test Reynolds number with Mach number for a model with 50° 38' sweptback wing, aspect ratio 2.98, taper ratio 0.45, and modified NACA 64A-series airfoil sections.

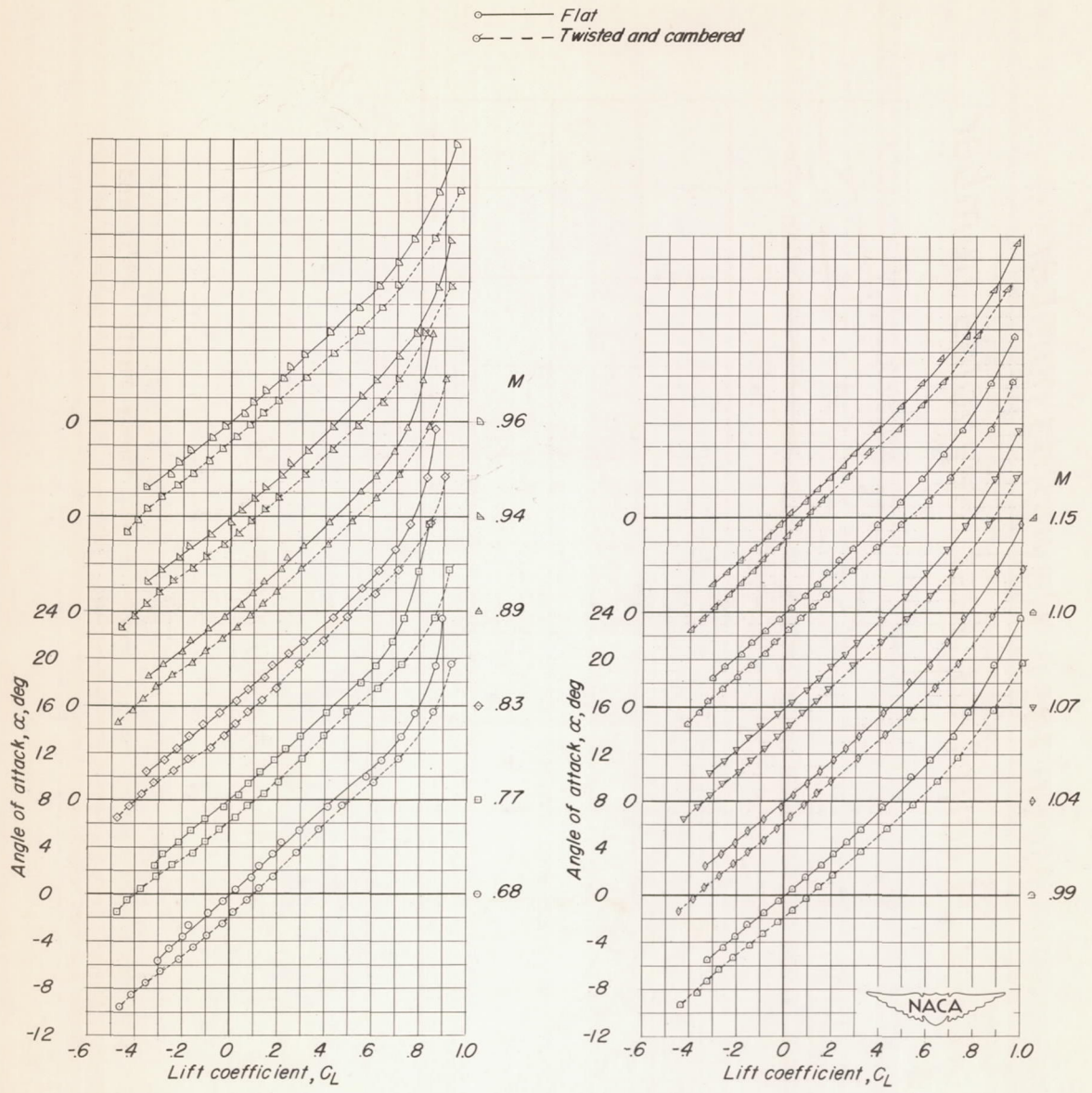

(a) α against C_L.

Figure 6.- Flat wing-alone and twisted and cambered wing-alone aerodynamic characteristics for the model with 50° 38' sweptback wings, aspect ratio 2.98, taper ratio 0.45, and modified NACA 64A-series airfoil sections.

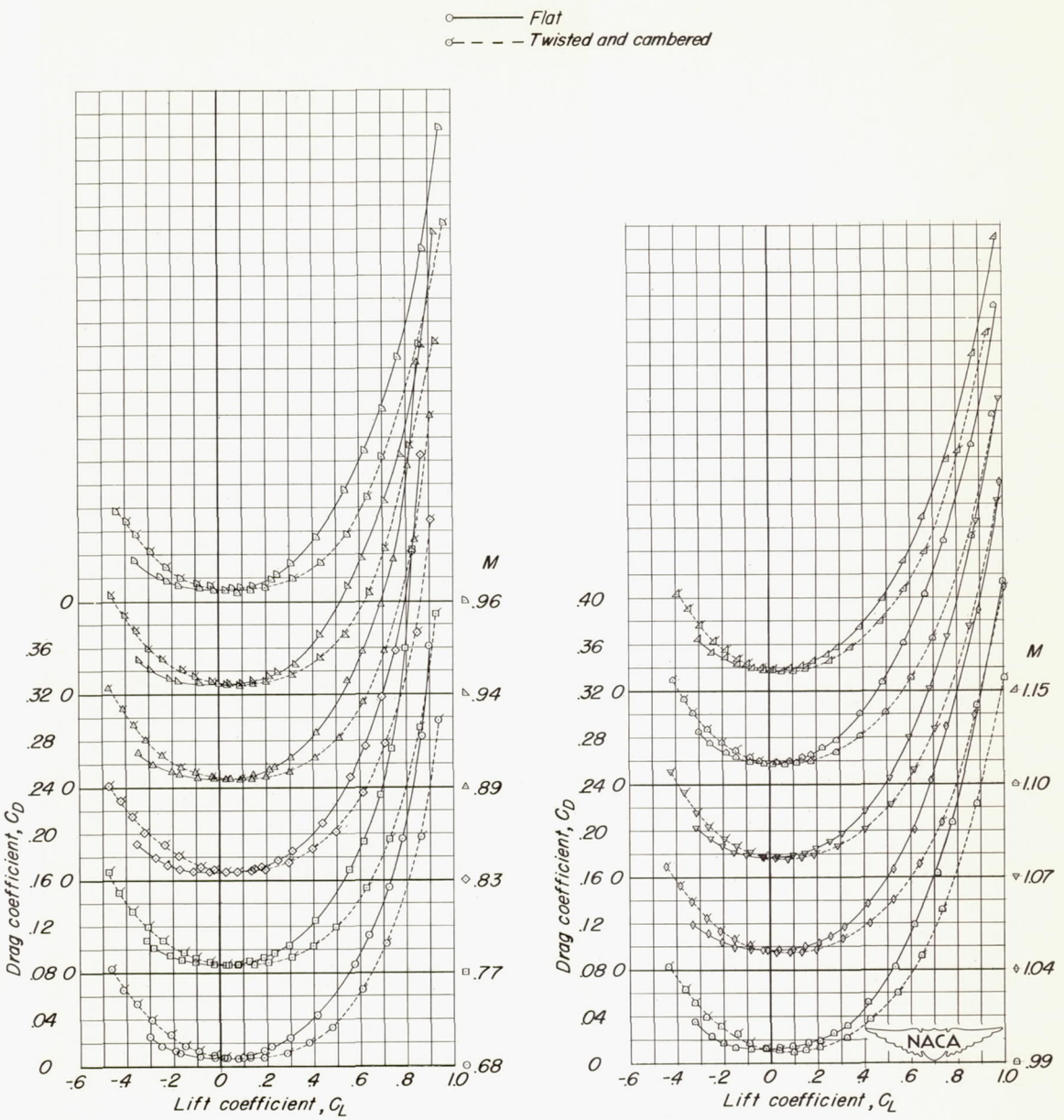

(b) C_D against C_L.

Figure 6.- Continued.

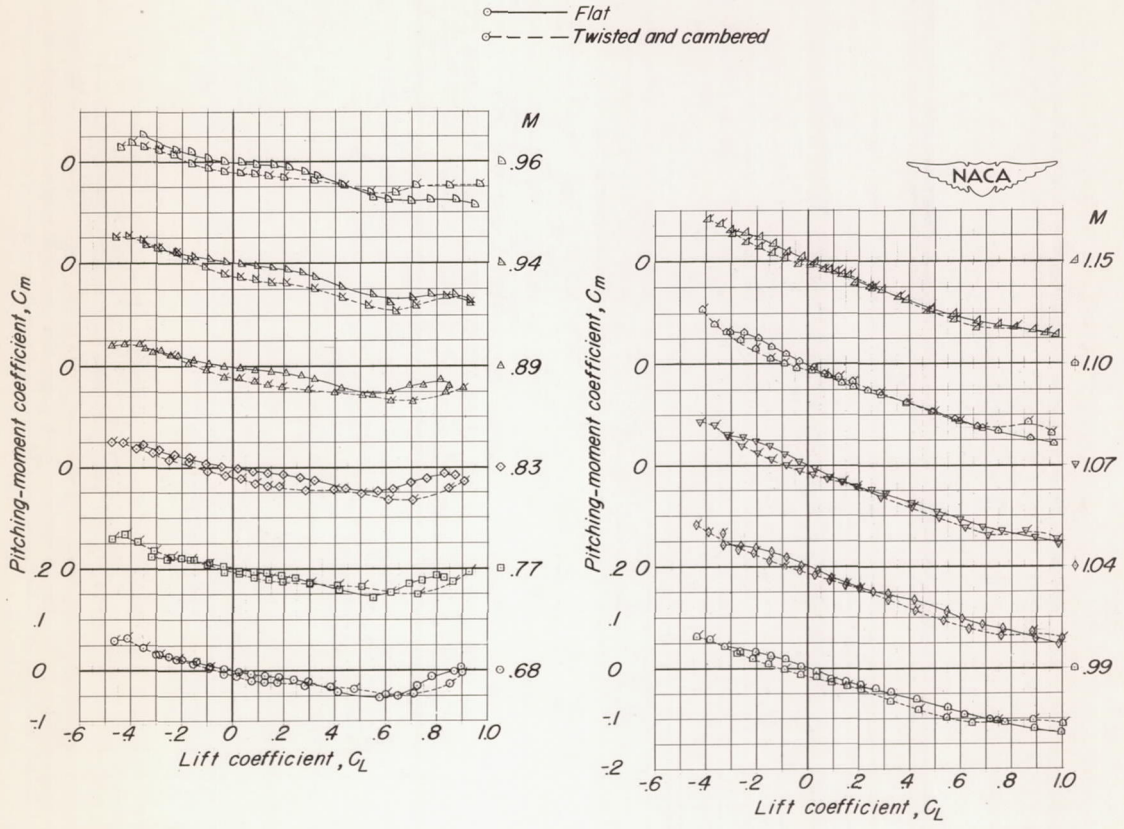

(c) C_m against C_L.

Figure 6.- Continued.

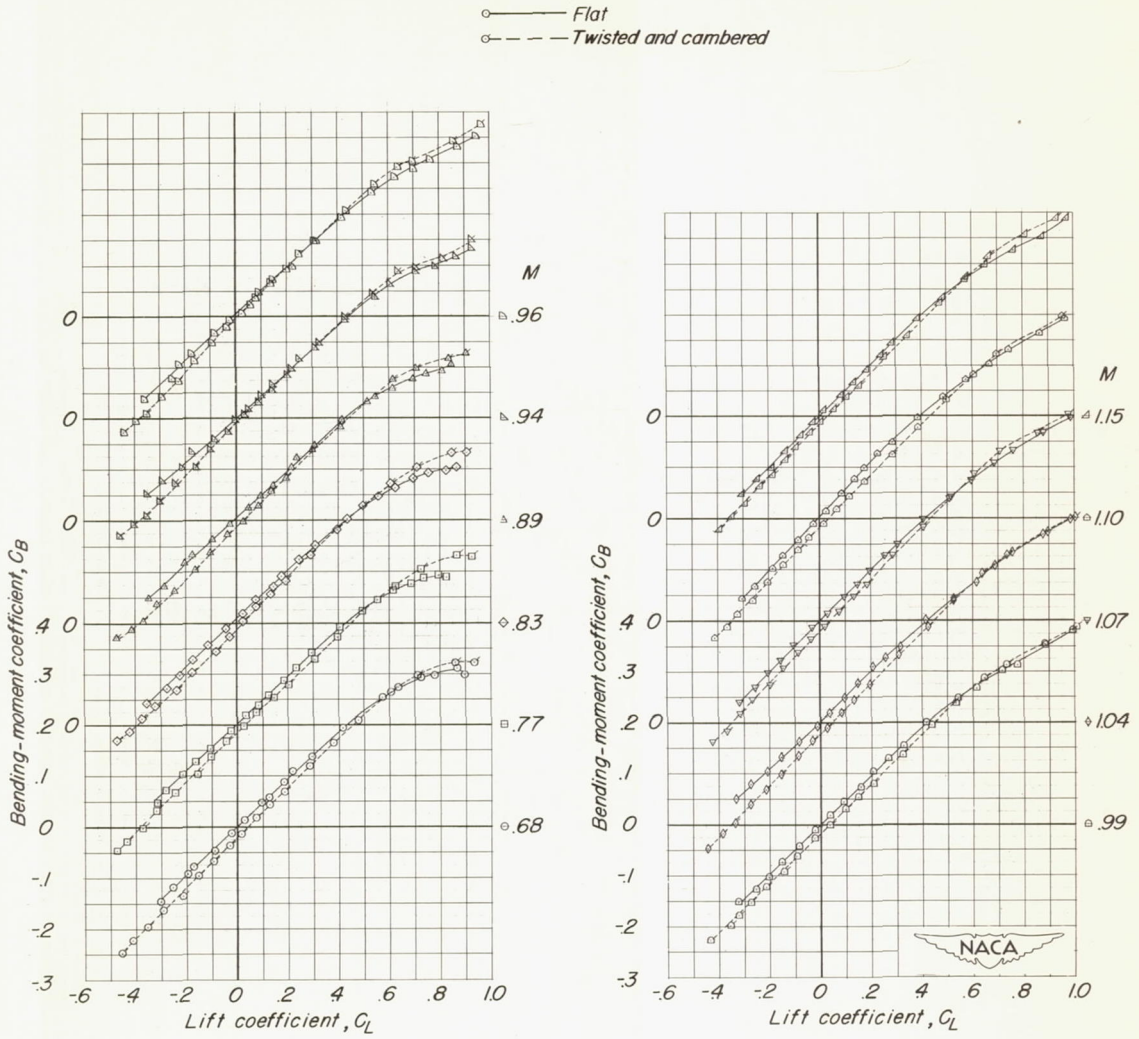

(d) C_B against C_L.

Figure 6.- Concluded.

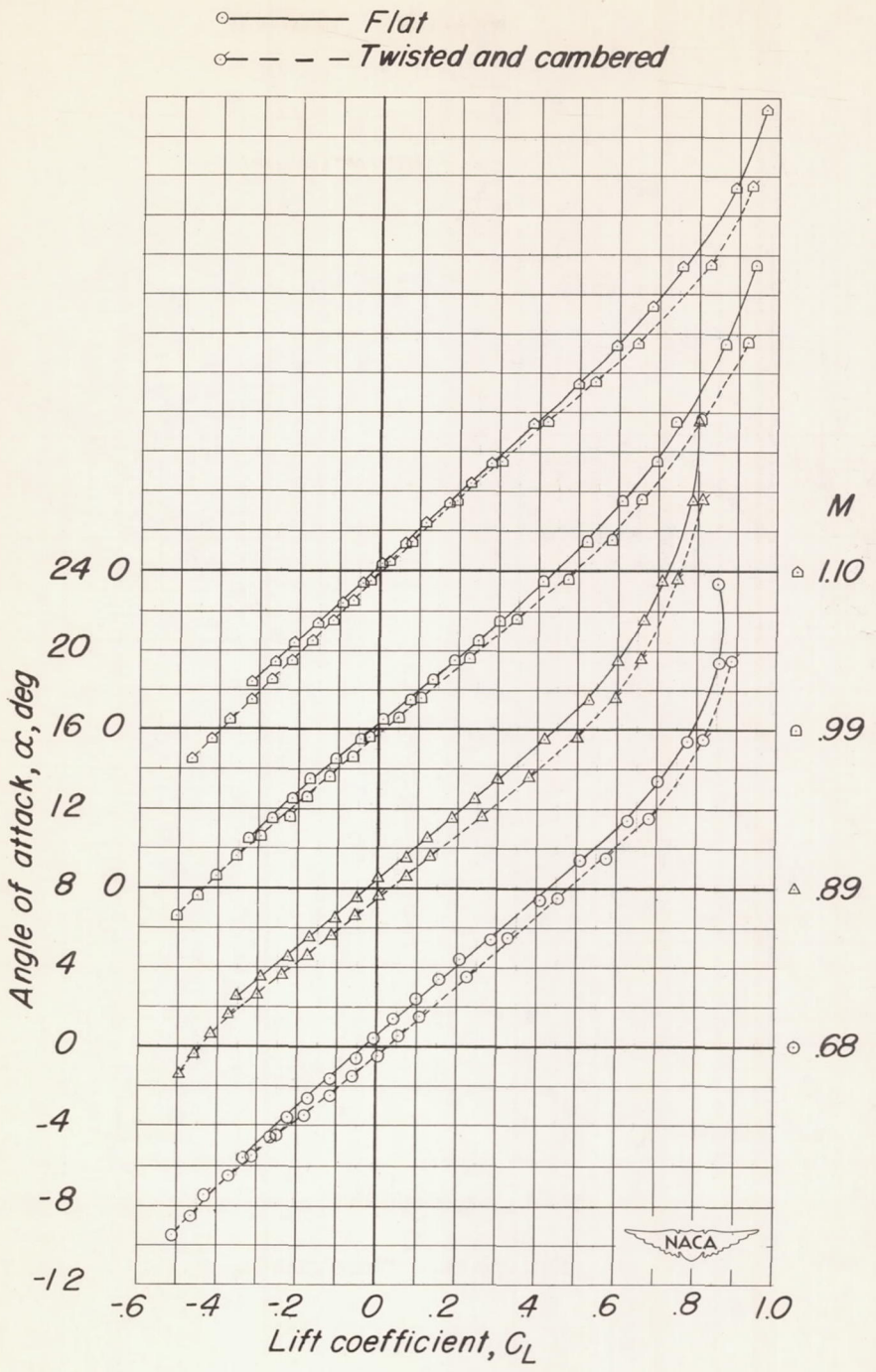

(a) α against C_L.

Figure 7.- Flat wing-fuselage combination and twisted and cambered wing-fuselage combination aerodynamic characteristics for the model with 50° 38' sweptback wings, aspect ratio 2.98, taper ratio 0.45, and modified NACA 64A-series airfoil sections.

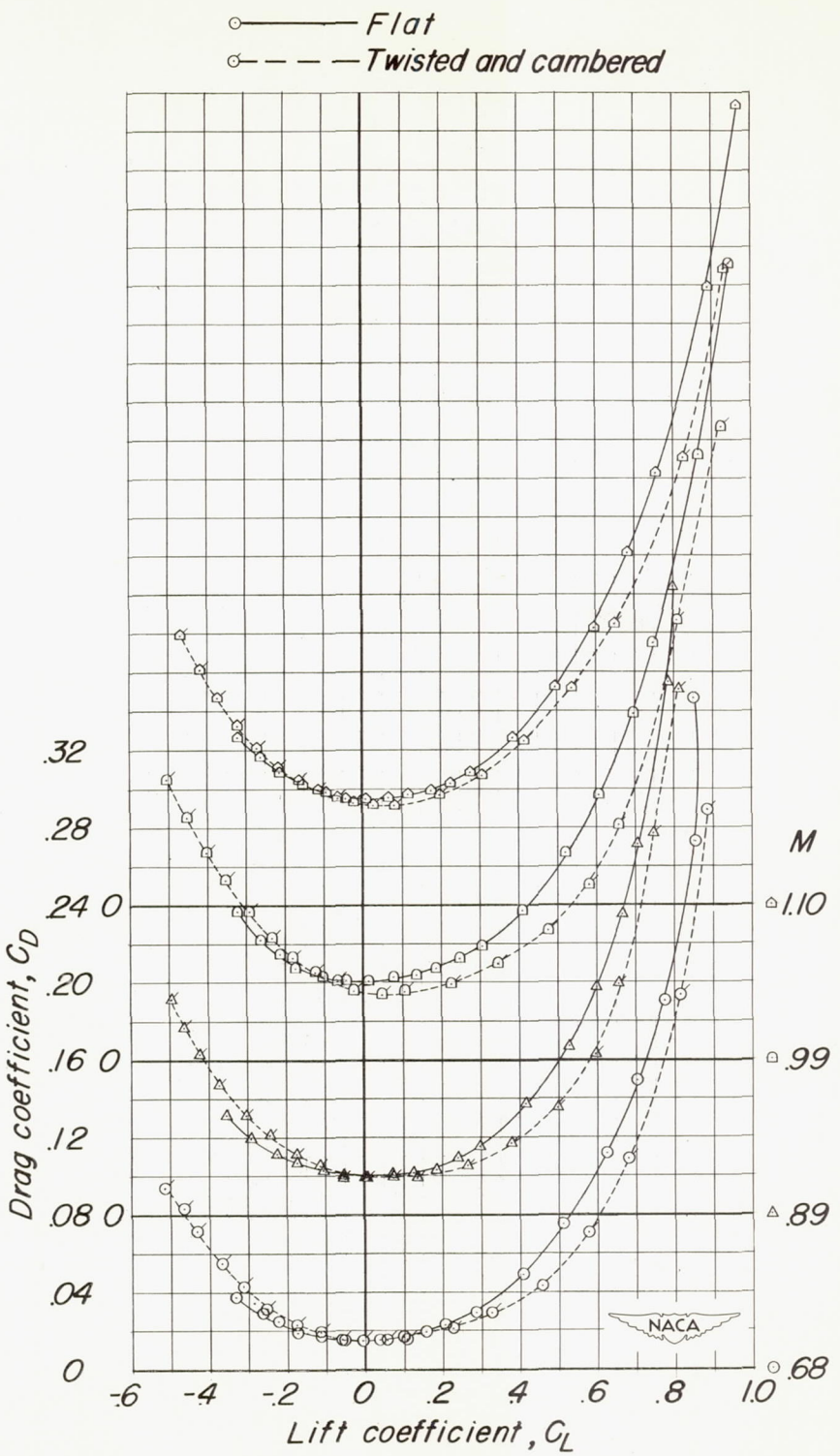

(b) C_D against C_L.

Figure 7.- Continued.

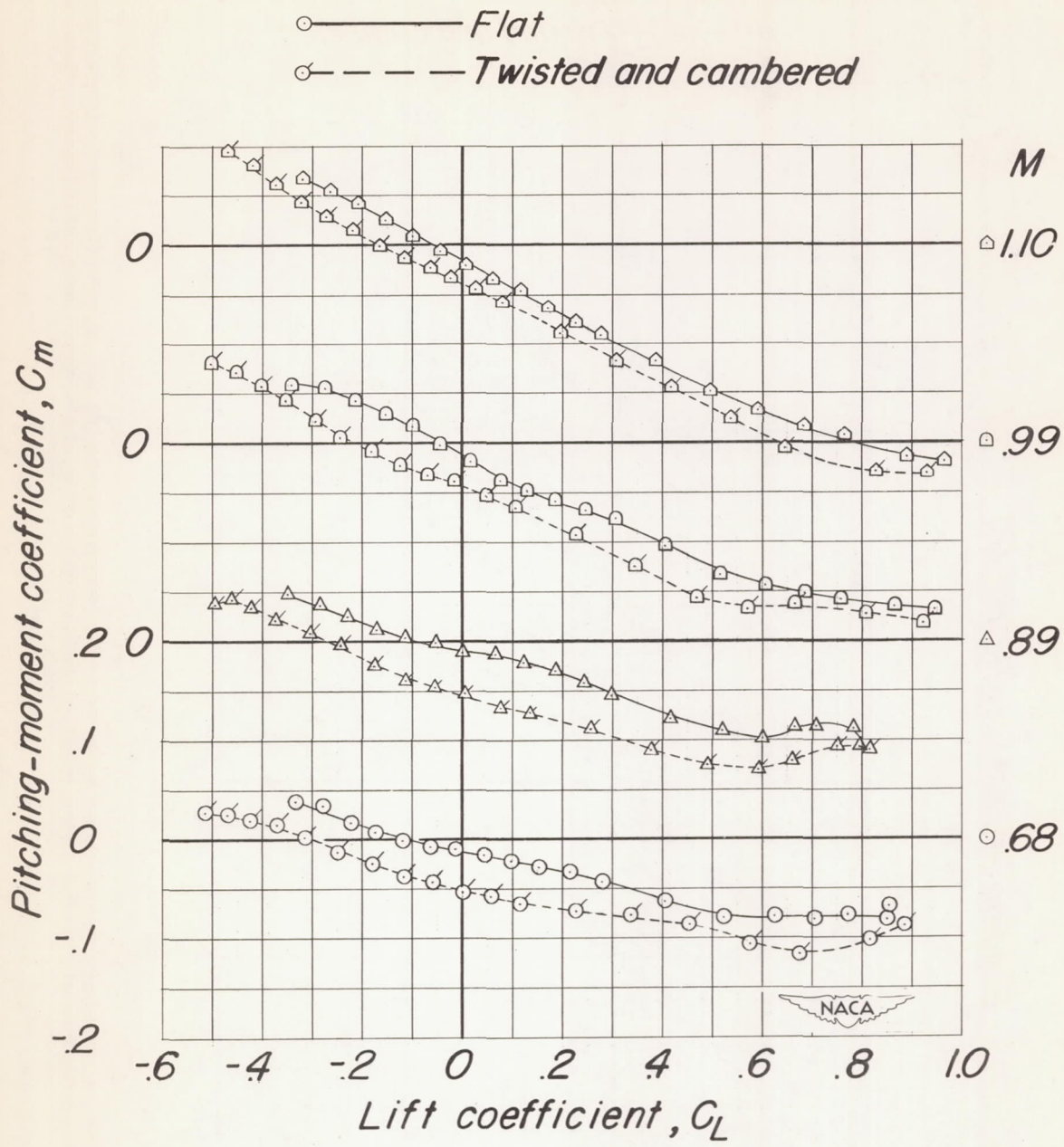

(c) C_m against C_L.

Figure 7.- Continued.

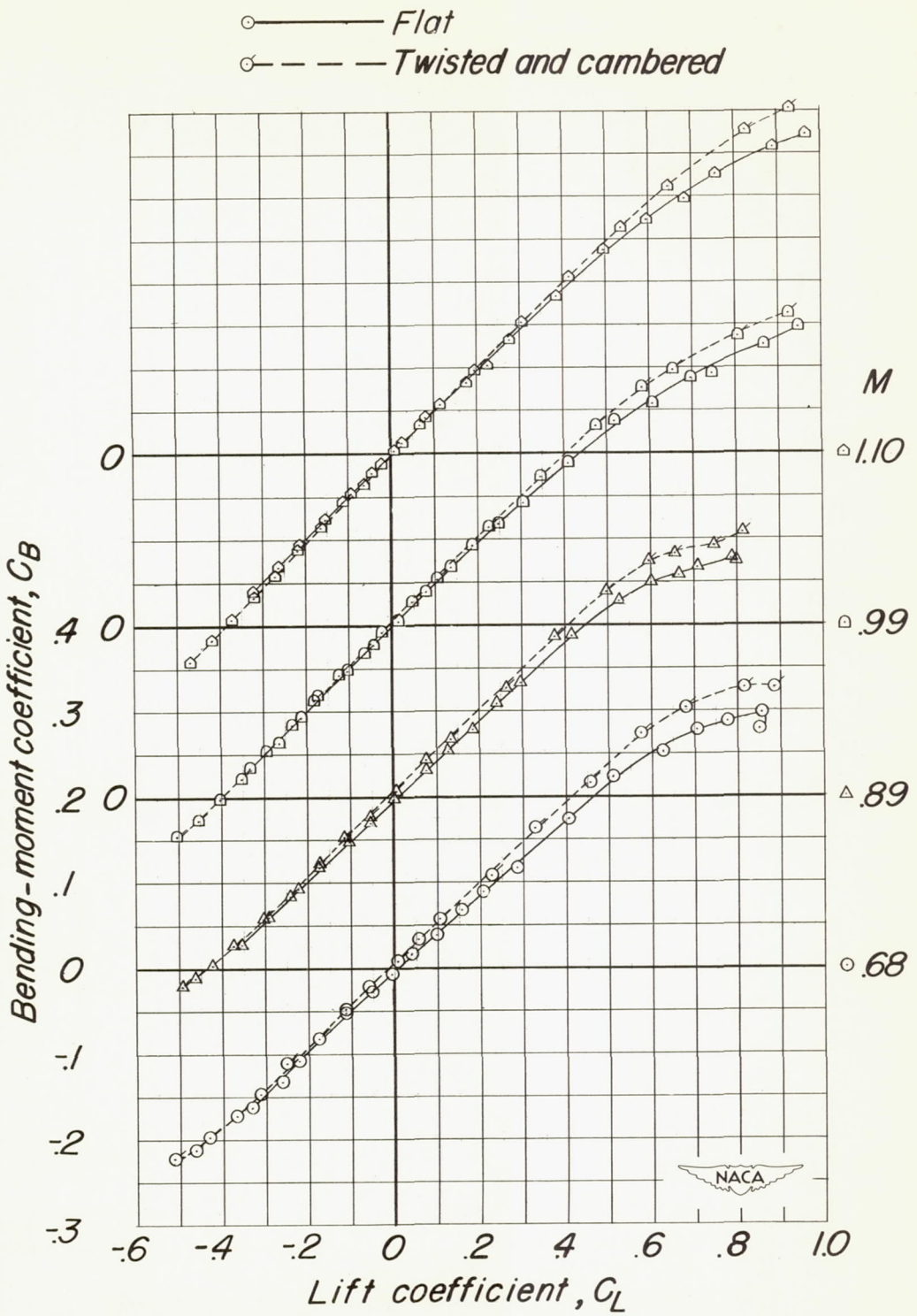

(d) C_B against C_L.

Figure 7.- Concluded.

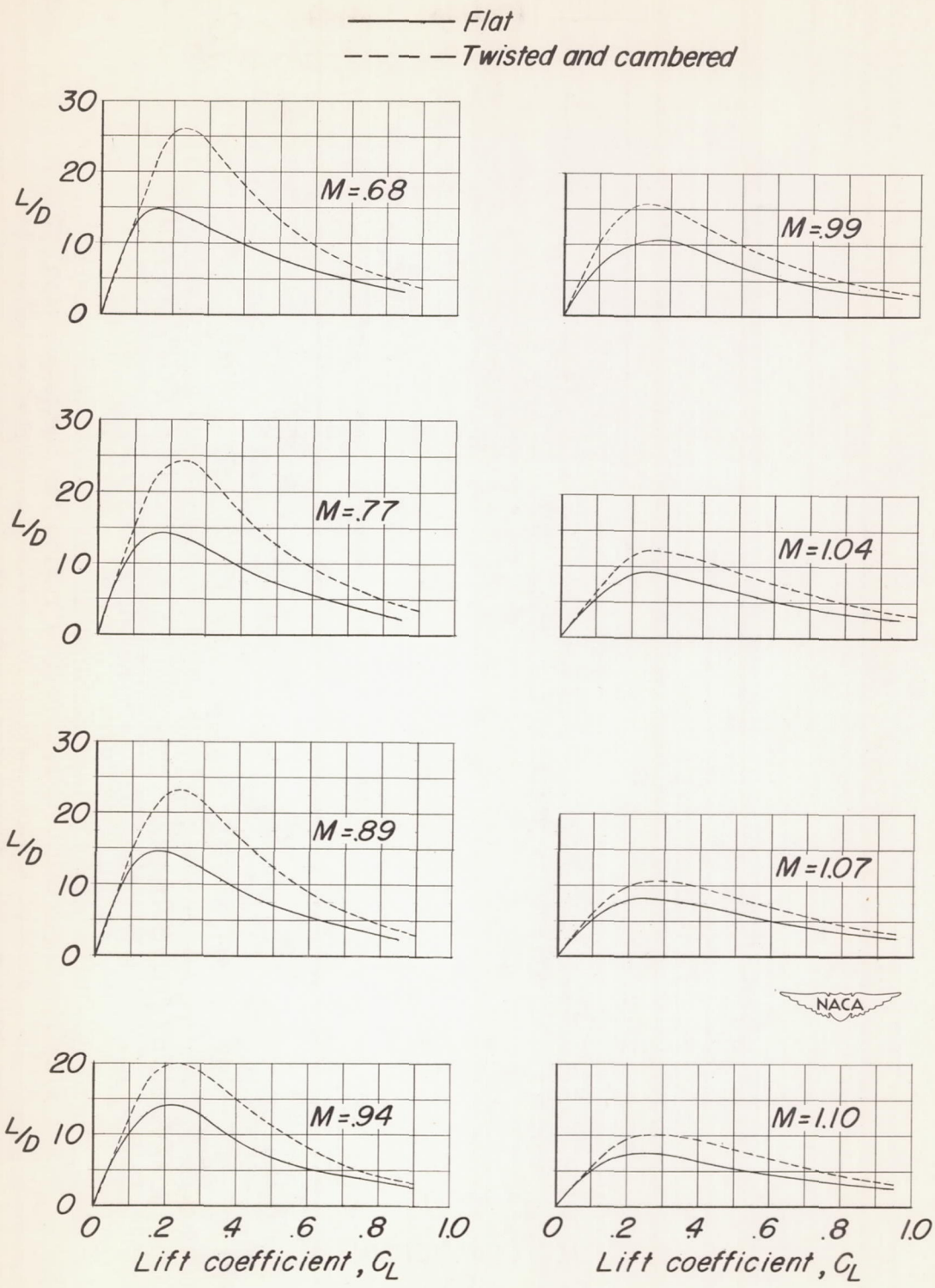

Figure 8.- Flat wing-alone and twisted and cambered wing-alone lift-drag ratios for the model with 50° 38' sweptback wings, aspect ratio 2.98, taper ratio 0.45, and modified NACA 64A-series airfoil sections.

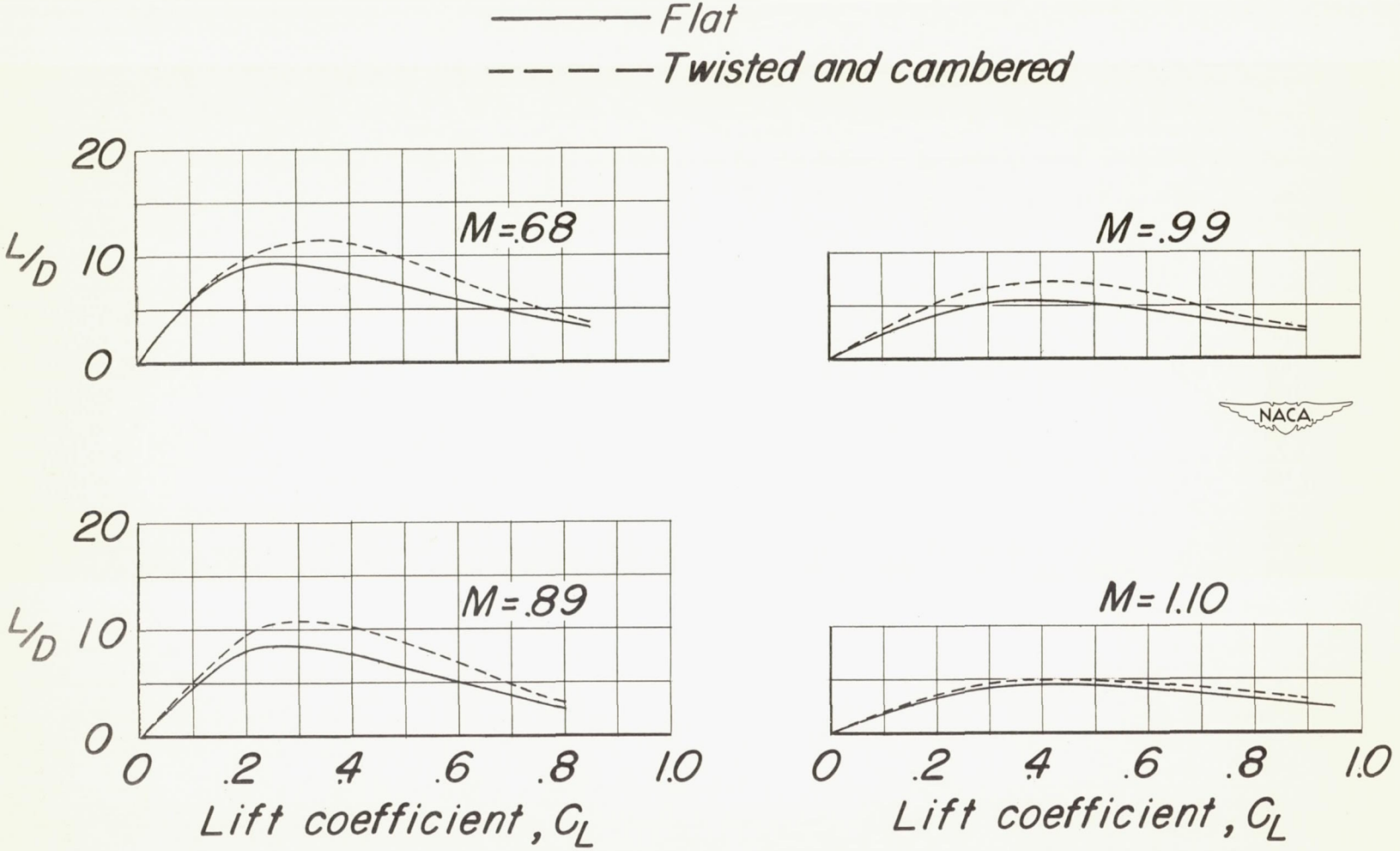

Figure 9.- Flat wing-fuselage combination and twisted and cambered wing-fuselage combination lift-drag ratios for the model with 50° 38' sweptback wing, aspect ratio 2.98, taper ratio 0.45, and modified NACA 64A-series airfoil sections.

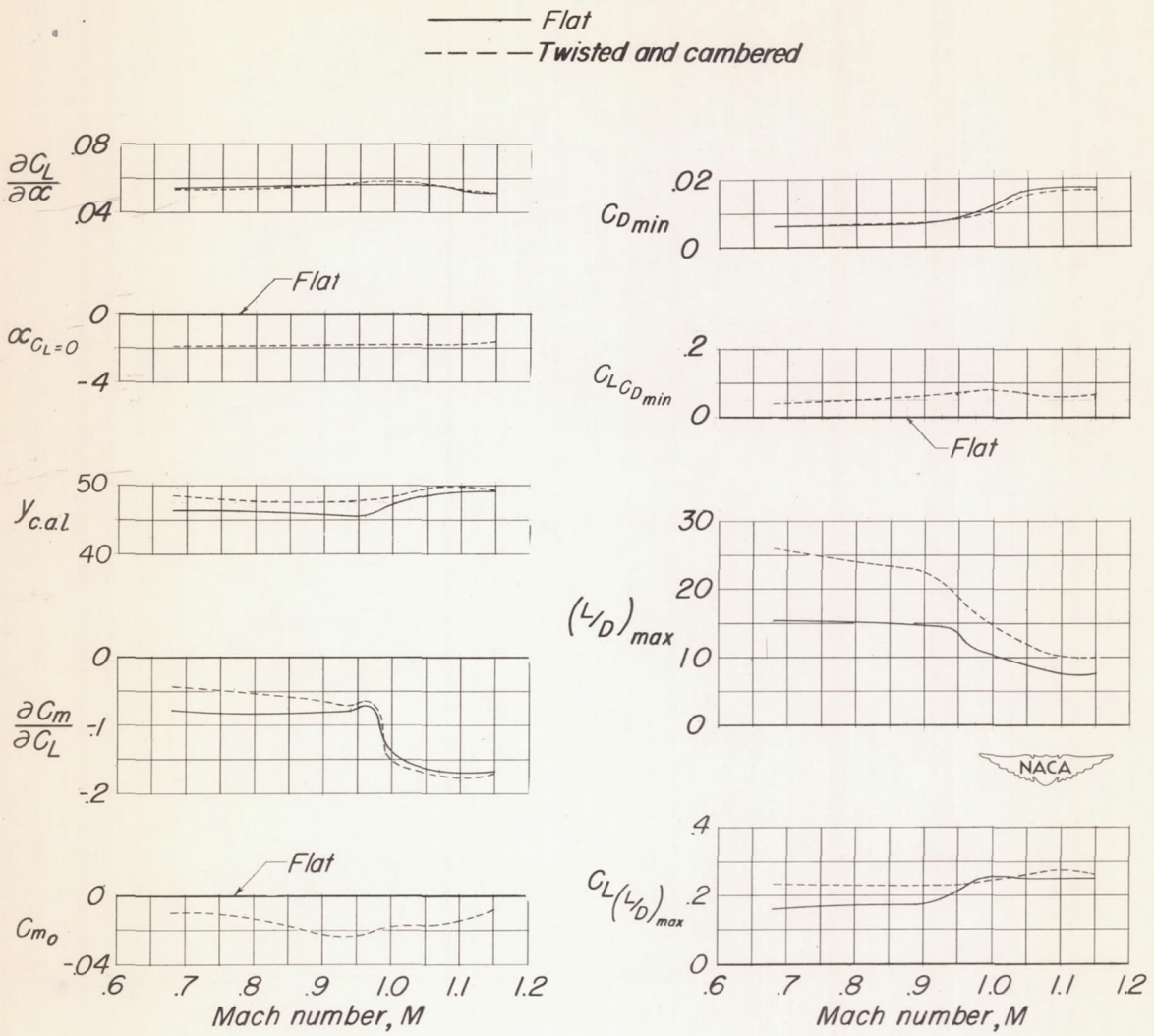

Figure 10.- Summary of aerodynamic characteristics of the flat wing alone and twisted and cambered wing alone for the model with 50° 38' swept-back wings, aspect ratio 2.98, taper ratio 0.45, and modified NACA 64A-series airfoil sections. (Slopes are averaged over lift-coefficient range of 0 to 0.4.)

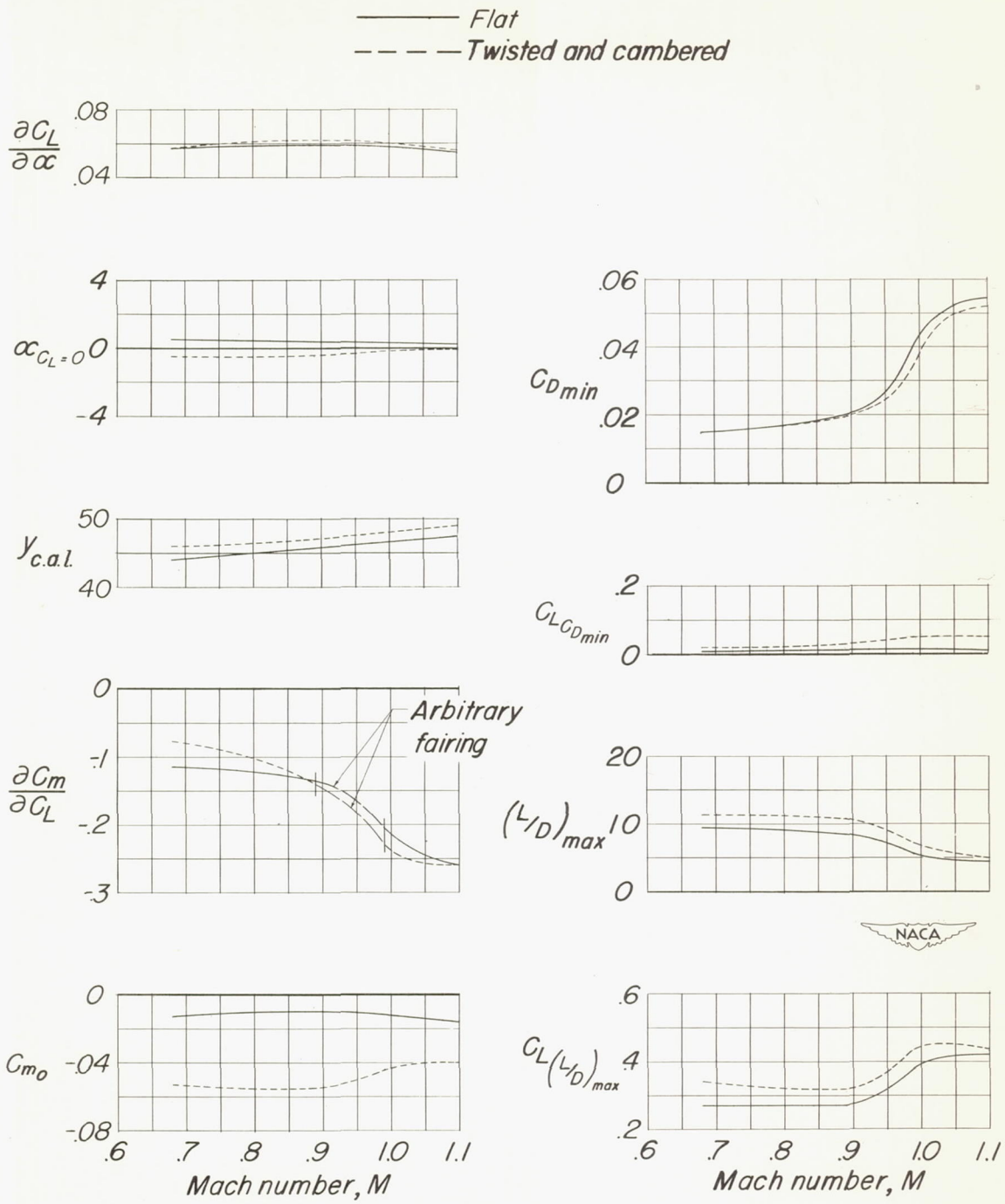

Figure 11.- Summary of aerodynamic characteristics of the flat wing-fuselage combination and twisted and cambered wing-fuselage combination for the model with 50° 38' sweptback wings, aspect ratio 2.98, taper ratio 0.45, and modified NACA 64A-series airfoil sections. (Slopes are averaged over lift-coefficient range of 0 to 0.4.)